JOURNAL OF MARINE SCIENCES & ENVIRONMENTAL TECHNOLOGIES
Vol. 5, Issue No. 2 (December-2019)

ISSN (Print): 2413-5267
ISSN (Online): 2706-9966

Finite Element Analysis of Free Energy Permanent Magnet Motor Using Solidworks and Finite Element Method Magnetics (FEMM) Software

Talal A. Elmasri[1, *], Mabrooka A. Elmasri[2], and Esra S. Abdulhafid[1]

[1)] Materials and Minerals Engineering Department, Faculty of Engineering, University of Ajdabiya, Ajdabiya, Libya.
[2)] Civil Engineering Department, Faculty of Engineering, University of Ajdabiya, Ajdabiya, Libya.

[*]**E-mail:** talal1876@yahoo.com

تحليل العناصر المحدودة (التفاضلية) لمحرك مغناطيسي ذاتي الدوران باستخدام برنامجي Solidworks و FEMM

طلال عبدالسلام المصري فضيل[1،*]، مبروكة عبدالسلام المصري فضيل[2] و إسراء صلاح عبدالحفيظ يونس[1]

[1)] قسم هندسة المواد والمعادن، كلية الهندسة، جامعة إجدابيا، إجدابيا، ليبيا.
[2)] قسم الهندسة المدنية، كلية الهندسة، جامعة إجدابيا، إجدابيا، ليبيا.

Received: 22 September 2019; Revised: 28 November 2019; Accepted: 15 December 2019

Abstract

These days, our environment is getting worse, and the emission of gas from non-renewable energy sources such as fossil fuel and coal is the main reason for the current environmental issue. Therefore, the development of new energy sources which is clean and non-polluted to the environment is getting more demand in our world today. Free energy sources such as magnet energy are adaptable in replacing non-renewable energy sources. A permanent magnetic generator is a free-energy instrument that gives off entirely free energy by using the energy stored in permanent magnets. Much research has been done in this area, but none of which precisely focused on the tradeoff of magnetic material in this application. Although plenty of different magnetic materials have been synthesized including nanomagnetic ones, it is not easy to select an optimal magnetic material for a certain technological application due to their properties confliction. In this study, a new design of free energy permanent magnet generator has been developed and significant simulations are being done by using Solidworks and Finite Element Method Magnetics (FEMM) software for simulation modeling in order to tradeoff among magnetic materials in terms of performance. Results show NdFeB 52 MGOe which are very strong magnets made from alloys of rare-earth elements offer an optimum performance of around 11,309.734 J per motor cell and 8 magnets of 28,696.92 size in mm3 for a disk of radius 20cm; however, they are so expensive and in limited supply. Alternatively, strong nanomagnetic materials have been synthesized to replace rare-earth-based magnets in different applications.

***Keywords**: Free energy permanent magnet generator, Rare-earth permanent magnets, Nanomagnetic materials, FEMM.*

الملخص

في هذه الأيام تتفاقم المشاكل البيئية وتزداد سوءًا، والمسبب الرئيسي في ذلك هي الغازات المنبعثة من مصادر الطاقة غير المتجددة مثل الوقود الأحفوري والفحم. لذلك فإن تطوير مصادر الطاقة المتجددة والنظيفة وغير الملوثة للبيئة أصبح طلباً ملحاً في عالمنا اليوم. مصادر الطاقة المجانية مثل طاقة

ISSN (Print): 2413-5267
ISSN (Online): 2706-9966

المغناطيس هي من ضمن مصادر الطاقة البديلة التي يمكن تبنيها كبديل لمصادر الطاقة التقليدية والملوثة للبيئة. المولد المغناطيسي هو أداة توفر الطاقة المجانية باستخدام الطاقة المختزنة على نحو ما في المغناطيس الدائم. تم إجراء العديد من الأبحاث في هذا المجال، ولكن لم يتم التركيز في أي منها على المفاضلة ما بين المواد المغناطيسية تحديداً. في عالم اليوم لدينا العديد من المواد المغناطيسية بما في ذلك المواد المغناطيسية النانوية والتي تُستخدم على نطاق واسع في التطبيقات التكنولوجية المختلفة. ومع ذلك من الصعب جداً تحديد المادة المغناطيسية المثالية لتطبيق ما من بين كل تلك المواد المغناطيسية المتوفرة والمصنعة بتقنيات مُختلفة بسبب التداخل على نطاق ضيق في على مستوى خواصها. في هذه الدراسة تم تطوير تصميم جديد لمولد مغناطيس ذاتي الدوران حيث تم إجراء عمليات محاكاة مهمة باستخدام برنامجي Solidworks و Finite Element Method Magnetics (FEMM) وذلك من أجل المفاضلة بين المواد المغناطيسية المدرجة في مكتبة البرنامج من حيث الأداء وإجراء كل الحسابات المطلوبة. أظهرت النتائج أن NdFeB 52 MGOe وهو مغناطيس قوي جدًا مصنوع من سبائك العناصر الأرضية النادرة قد يوفر أداءً مثاليًا يُقدر بحوالي 11,309.734 جول من الشغل المنجز لكل (خلية محرك) ذات 8 مغناطيسات بحجم 28,696.92 مم^3 مُثبتة على قرص قطره 20 سم. إلا أن هذا النوع من المغناطيسات الدائمة والتي تُسمى مغناطيسات النوديوم هي مكلفة للغاية وتوريدها متوفر بكميات محدودة. لذلك وُجدت المواد المغناطيسية النانوية القوية وذات الخواص المغناطيسية المقاربة لخواص مغناطيسات النوديوم لتحل محلها في تطبيقات مختلفة.

الكلمات الدالة: مولد مغناطيسي ذاتي الدوران، مغناطيسات العناصر الأرضية النادرة، المغناطيسات النانوية.

1. Introduction

Traditional energy generators continuously consume large amount of fossil fuels that is depleted, emitted in atmosphere and destroy the environment. Therefore, the development of new energy sources which is clean and non-polluted to the environment is getting more demand in our world today. A permanent magnetic generator is a free energy instrument that gives off entirely free energy by using the energy stored in permanent magnets that can be reliably used to replace the traditional ones. Many researches have been done in this area, but none of which precisely focused in tradeoff of magnetic material in this application. Although plenty of different magnetic materials have been synthesized including nanomagnetic ones, it is not easy to select an optimal magnetic material for a certain technological application due to their properties confliction. Rare-earth permanent magnets (e.g.) are very strong magnets made from alloys of rare-earth elements and obviously offer an optimum performance particularly in the permanent magnetic motor application, although they are so expensive and in limited supply. Alternatively, strong nanomagnetic materials have synthesized to replace rare-earth-based magnets in different applications. The main purpose of this paper is to tradeoff among magnetic materials in order to improve performance of free energy magnetic generators. Creating a new design of a permanent magnetic motor is to be considered in this study by using CAD software (Solidworks and FEMM) for simulation.

Gathering energy from the surrounding environment without burning a fuel or coal represents the general definition of the term "Free-Energy". Free energy is coming from the local environment that supply to the system where these free energy is indefinite and perpetual. However, the conventional science contradicts the method of free energy. Conservation of energy law shows that no more output energy can be taken out of a system than the input supplied energy to the system, and this undoubtedly correct fact has not been broken (Kelly, 2010).

ISSN (Print): 2413-5267
ISSN (Online): 2706-9966

Magnetic materials are sorted into the following categories: Ferromagnetic, antiferromagnetic ferrimagnetic, diamagnetic, and paramagnetic materials. This classification is based on the behavior of magnetic material when they exposed to an external magnetic field. As a result of the magnetic field exposure, a net magnetic moment at the atomic level that opposes the applied magnetic field is generated. Alignment, interaction and coupling those magnetic moments as a response to the applied field, determine how weak or strong the magnetic material is. For instance, the coupling of the net magnetic moments is weak in case of paramagnetic materials, whereas it is a strong coupling at ferromagnetic. Regions of coupling called domains of the net magnetic moments are spontaneously aligned parallel or antiparallel to one another and consequently set the magnetic properties of the material (Furlani, 2001).

The addition of 5% copper to Permalloy which is an easily magnetized and demagnetized alloy results in an alloy called MU-Metal. Commercially, 2% Cr is also introduced in MU-Metal alloy. Because of its more ductility over Permalloy, MU-Metal can be formed into thin sheets to be used as a protective magnetic shielding of sensitive electronic components from stray magnetic fields (Jiles, 1991).

Finite Element Method Magnetics (FEMM) is an accurate simple and popular software package for simulating and solving both permanent and electromagnetic problems. Linear and nonlinear harmonic low frequency magnetic and magnetostatic problems and linear electrostatic problems could be addressed in 2D planar and 3D axisymmetric (Baltzis, 2010).

2. Methodology

Several procedures and methods were used in this study in order to come out with a successful self-rotating free energy motor based on permanent magnets. A simulation and modeling were done for a new design of the motor by using Solidworks and FEMM software in three successive steps, designing, SolidWorks drawing, and FEMM simulation. The motor design was created based on repulsive forces between trapezoidal cross-section magnets (Figure 1.a) that reversely arranged in circular pattern on a movable and stationary disks as shown in Figure 1b and Figure 1c respectively. A Solidworks drawing and assembly of the design displayed in Figure 1d which consists of one stationary and two movable disks concentric in a shaft, and a ball bearing fixed in the stationary disk center to allow the shaft movement. This assembly represents a cell of the design that could be linearly repeated. The trapezoidal shape of magnets enables the movable disks to rotate in the same direction under the repulsion effect of stationary disk magnets as simply clarifying in Figure (2). MU Metal was proposed in the design in order to shield magnets and prevent unneeded interactions between magnets during rotation.

ISSN (Print): 2413-5267
ISSN (Online): 2706-9966

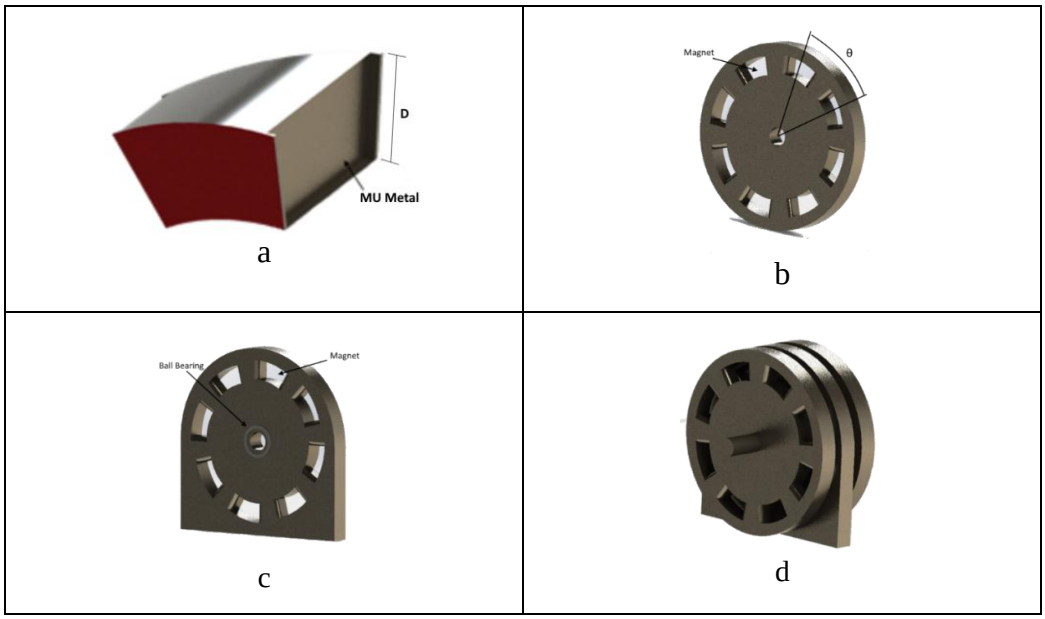

Figure 1. 3D rendering of the model and its main components

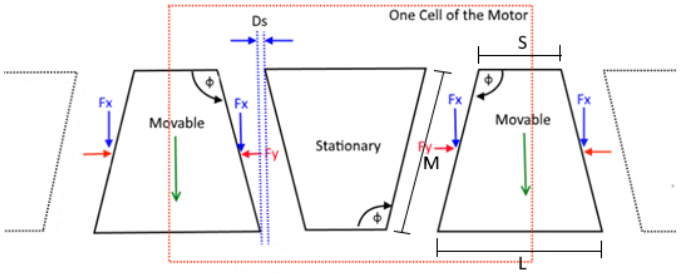

Figure 2. Top view drawing of the stationary and movable magnets

Trapezoidal shapes were drawn for convenience by using Solidworks 2012 in spite of they could be done on FEMM with many steps which would be time consuming. Figure (3) shows a sample of trapezoidal shape was drawn by using Solidworks 2012, which is a magnet placing in a medium of air saved in DXF file format (FEMM supported).

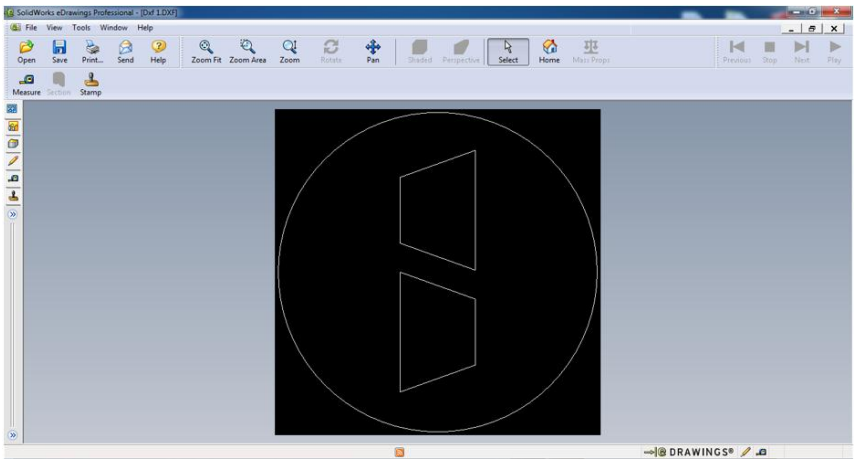

Figure 3. Representation of DXF file format

ISSN (Print): 2413-5267
ISSN (Online): 2706-9966

Several (2-D) simulation steps were done by using FEMM software with a view to calculating the components of the repulsive force between magnets in horizontal (F_x) and vertical (F_y) directions for further considerations and computations. Figure (4) shows the calculated horizontal and vertical components of the repulsive force as a final result of fifteen simulation steps.

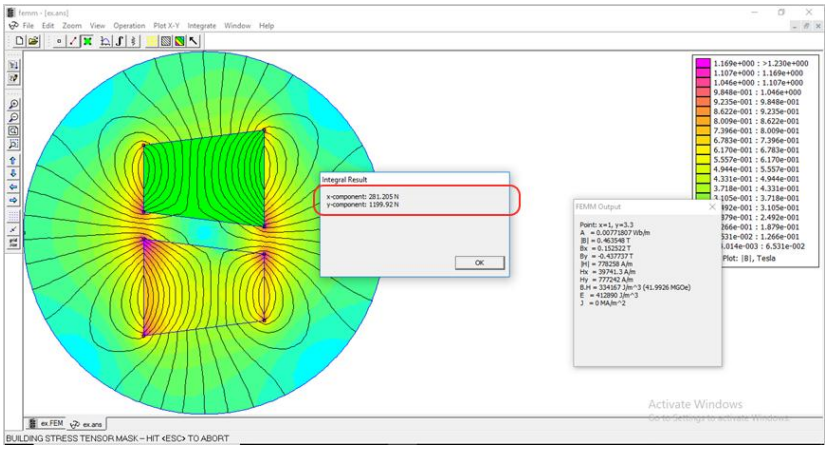

Figure 4. Showing the final result of the repulsive force components

A magnetic material's type from FEMM materials library had been simulated at different contact angles (Φ) and at constant separation distance (Ds) and depth (D) (Figure 2) so as to calculate the optimum contact angle at which the horizontal repulsive force component was maximum. Then at the optimum found contact angle and a constant depth, a magnetic material's type from FEMM materials library was simulated at different separation distances in order to display the horizontal repulsive force component changes. Furthermore, the horizontal repulsive force component had been simulated at the optimum contact angle and separation distance of different depths. Then it was repeated for three different cross-sectional areas of magnets. Moreover, it had been simulated at the same optimum conditions and at different cross-sectional areas of magnets. Then it was repeated for three different depths. Finally, all magnetic materials of FEMM materials library were simulated at the optimum found conditions to present the horizontal repulsive force component alterations.

The calculated repulsive force between magnets during rotation does not act suddenly and once a time; however, it takes place once the magnets start contacting. It gradually reaches its maximum value when the magnets become at a completely contact position, and then it decreases in the same way as magnets are rotating away from each other. The increasing and decreasing relations pattern had been estimated and based on which the cumulated value of the horizontal repulsive force component was calculated.

The work done in rotational displacement was computed by using the following formula:

$$W = T \times \theta \qquad \ldots\ldots\ldots \quad (1)$$

Where (T) is the Torque (N·m) which is generated by a couple of horizontal repulsive force components ($2F_x$) multiply by the movable disk radius (r), and (θ) is step angular

ISSN (Print): 2413-5267
ISSN (Online): 2706-9966

displacement expressed in radians. Eqn. (1) is valid for the work done finding of a force couple per an angular displacement step, whereas the design configuration shows eighth ones were allocated one force couple to each one-eighth of the disk circumference (Figure 2). A modified equation of the aforementioned work done formula was generally expressed in Eqn. (2), where (n) is number of angular displacements or couples.

$$W = T \times n \times \theta \quad \ldots\ldots\ldots \quad (2)$$

The motor cells could be linearly repeated to gain more energy by multiplying the acting force couples on both of the movable disk sides as illustrates in Figure (2). Eqn. (2) calculates the work done on one side of the movable disk. Therefore, the work done acting on both sides was duplicated and estimated in relation to number of cells.

3. Results

Findings obtained from the simulation and modeling were displayed, analyzed and discussed in this part of the study. Even though both of the repulsive force components have been simulated, the vertical one was provided as annexes data. Labeling of a trapezoidal shape dimensions represents the cross-sectional view of magnets under consideration is shown in Figure (2). The (Φ vs. F_x) variation results summarized in Table (1). Figure (5) provides an overview of the optimum (Φ) simulation results at which (F_x) was maximum. Besides, the (Ds vs. F_x) simulation results were listed in Table (2).

Table 1. Tabulation of the (Φ vs. F_x) results

NdFeB 52 MGOe, **L**: 60 mm, **M**: 40 mm, **Ds:** 1mm, and **D:** 25.4 mm			
SN	**Angle (Φ^O)**	**Force (N)**	
		F_x	**F_y**
1	106	80.7073	275.133
2	107	81.3779	262.695
3	108	81.9075	250.909
4	109	82.0771	238.796
5	109.6	82.2531	231.397
6	109.7	82.8322	230.785
7	109.8	82.2674	229.669
8	110	81.2287	227.638

ISSN (Print): 2413-5267
ISSN (Online): 2706-9966

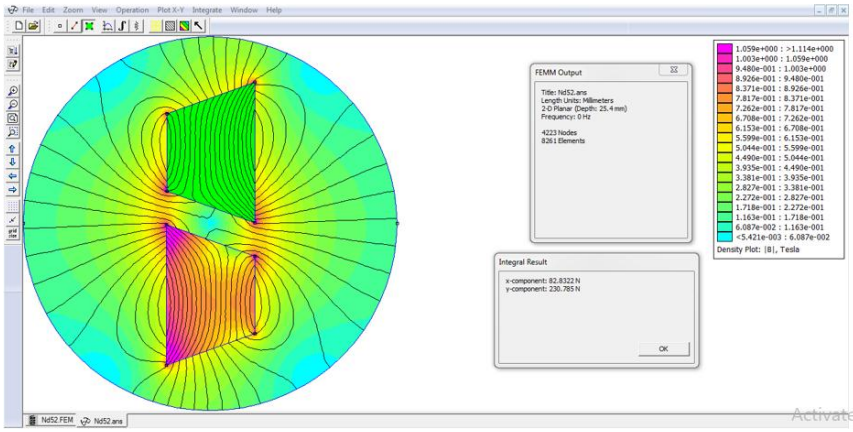

Figure 5. Overview of the optimum Φ results

Table 2. The results of F_x variation with Ds

NdFeB 52 MGOe, **L**: 60 mm, **M**: 40 mm, **Φ:** 109.70 °, and **D:** 25.4 mm			
SN	**Ds (mm)**	**Force (N)**	
		F_x	**F_y**
1	1.0	82.8322	230.785
2	1.1	80.6371	230.369
3	1.2	80.4385	229.933
4	1.3	80.1964	229.899
5	1.4	79.5616	229.844
6	1.5	78.9049	229.011
7	1.6	78.8026	228.72
8	1.7	78.3911	228.52
9	1.8	77.7271	228.256
10	1.9	77.0998	227.456
11	2.0	76.8605	227.195

Table (3) presents (F_x) and (F_y) values at various (L) for three multiples of (D), which were graphically illustrated in Figure (6). Figure (7) shows a sample of the results in which (F_x) was the highest than others. Furthermore, Table (4) outlines (F_x) variation due to (M) changing for three multiples of (D) that were graphically displayed in Figure (8). The highest simulated value of (F_x) was shown as a sample in Figure (9).

ISSN (Print): 2413-5267
ISSN (Online): 2706-9966

Table 3. The results of F_x vs. L for three multiples of D

NdFeB 52 MGOe, **Φ**: 109.7°, **M**: 40 mm, and **Ds:** 1 mm			
SN	**L (mm)**	**Force (N)**	
		F_x	**F_y**
		D_1 = 25.4 mm	
1	90	80.3233	281.414
2	100	80.2408	291.562
3	150	79.8159	320.503
		D_2 = 50.8 mm	
1	90	160.647	562.828
2	100	160.482	583.124
3	150	159.632	641.006
		D_3 = 76.2 mm	
1	90	240.97	844.242
2	100	240.723	874.686
3	150	239.448	961.508

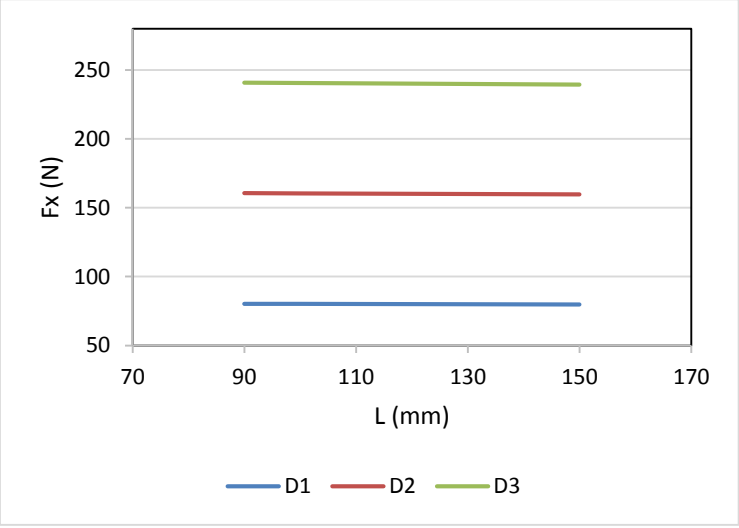

Figure 6. Variation of F_x with L at multiples of D

ISSN (Print): 2413-5267
ISSN (Online): 2706-9966

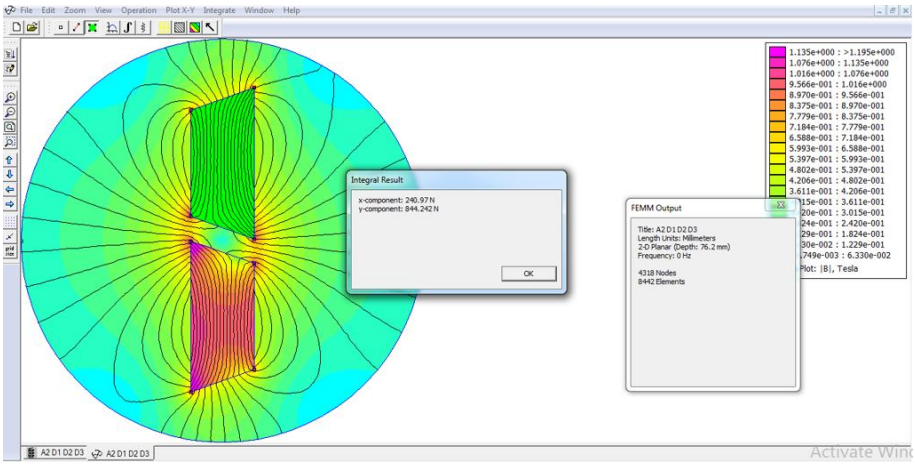

Figure 7. Overview of the highest F_x vs. L results provided as a sample

Table 4. The results of Fx vs. M for three multiples of D

NdFeB 52 MGOe, Φ: 109.7°, **L**: 150 mm, and **Ds:** 1 mm			
SN	**M (mm)**	**Force (N)**	
		F_x	**F_y**
		D_1 = 25.4 mm	
1	50	102.17	383.81
2	60	123.413	437.532
3	70	146.253	486.165
		D_2 = 50.8 mm	
1	50	204.34	767.619
2	60	246.827	875.064
3	70	292.506	972.33
		D_3 = 76.2 mm	
1	50	306.51	1151.43
2	60	370.24	1312.6
3	70	438.759	1458.49

ISSN (Print): 2413-5267
ISSN (Online): 2706-9966

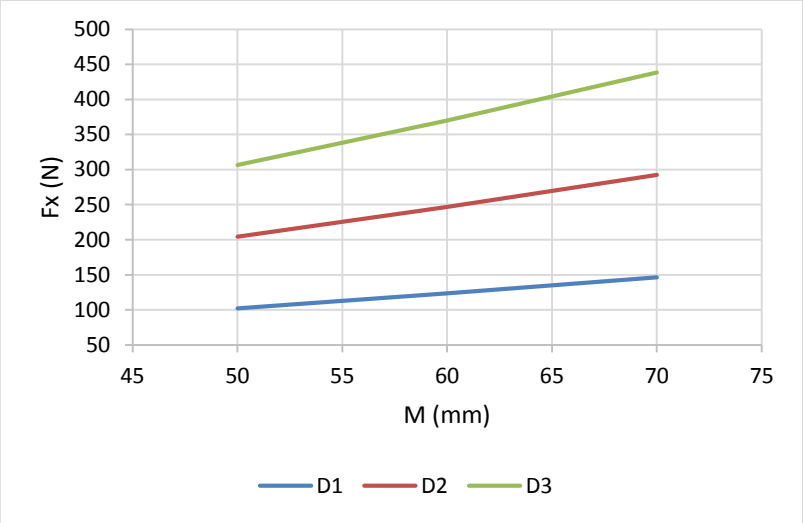

Figure 8. Variation of F_x with M at multiples of D

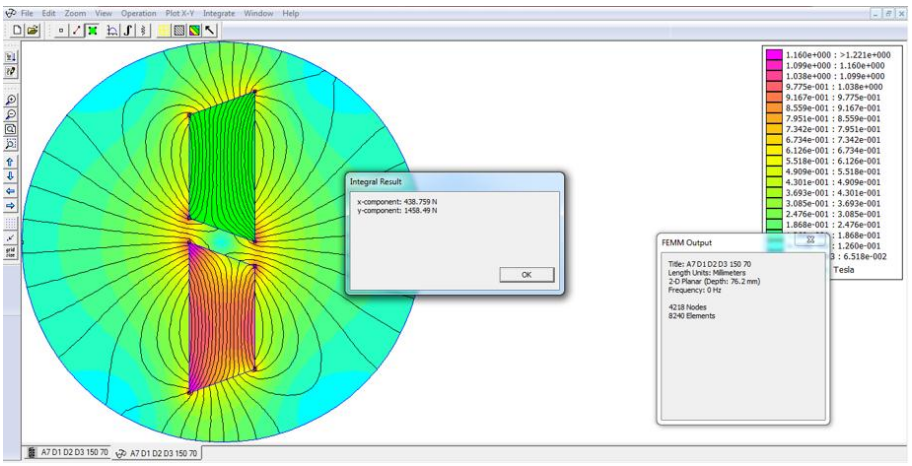

Figure 9. Overview of the highest F_x vs. M results provided as a sample

Table (5) outlines the results of (F_x) and (F_y) for various magnetic materials available in FEMM software's materials library. Figure (10) shows the graphical results of neodymium magnets. Moreover, NdFeB 52 MGOe was simulated at (D= 25.4 mm, Ds= 1 mm, Φ= 109.70, L= 60 mm, and M= 40 mm) of single-sided and double-sided shielding using MU metal with different thickness from 5 mm up to 26 mm. Figures (11 and 12) were displayed as samples of single and double sided shielded magnets respectively.

ISSN (Print): 2413-5267
ISSN (Online): 2706-9966

Table 5. The results of F_x for different magnetic materials

L: 60 mm, **M:** 40 mm, **Ds:** 1 mm, **Φ:** 109.70°, and **D:** 25.4 mm			
SN	**Magnetic material's type**	**Force (N)**	
		F_x	**F_y**
NdFeB Magnets			
1	NdFeB 52 MGOe	82.8322	230.785
2	NdFeB 40 MGOe	60.8548	196.098
3	NdFeB 37 MGOe	57.2316	184.521
4	NdFeB 32 MGOe	49.2933	159.183
5	NdFeB 10 MGOe	15.3357	45.3964
SmCo Magnets			
1	SmCo 27 MGOe	40.3852	126.54
2	SmCo 24 MGOe	35.8093	111.809
3	SmCo 20 MGOe	29.9423	97.2424
Ceramic Magnets			
1	Y30	6.3617	15.6245
2	Ceramic 5	5.78409	13.8877
3	Ceramic 8	5.69875	15.7786
4	Y25	5.45391	10.6631
Alnico Magnets			
1	Alnico 8	4.8277	6.40126
2	Alnico 6	2.11891	2.1185
3	Alnico 5	1.62804	1.54232

ISSN (Print): 2413-5267
ISSN (Online): 2706-9966

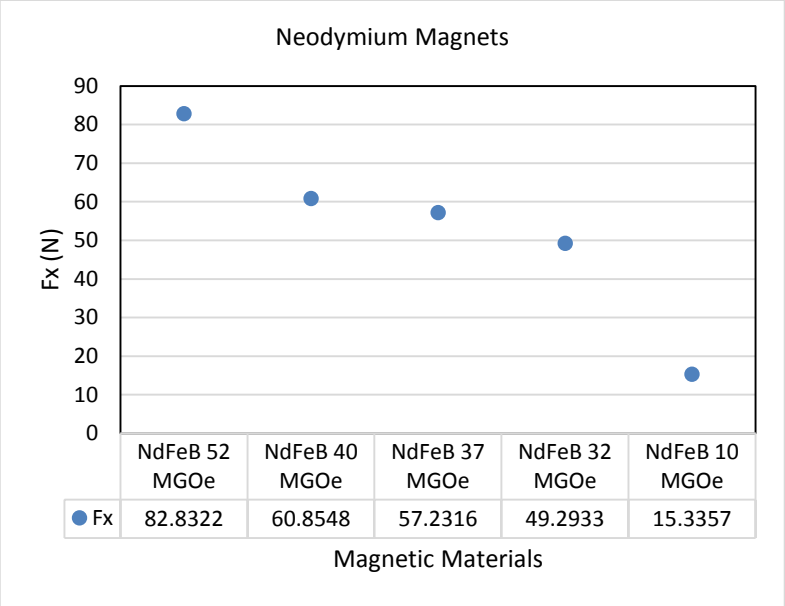

Figure 10. The results for neodymium magnets

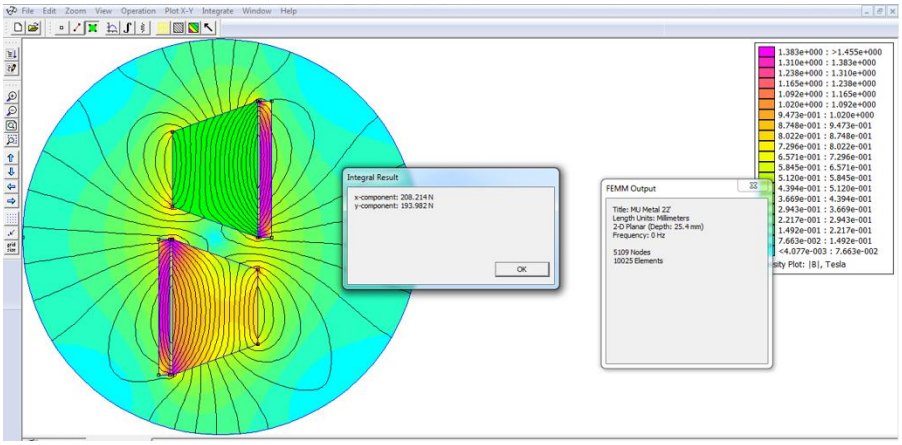

Figure 11. The results of single-sided shielding with 5mm MU Metal Thickness

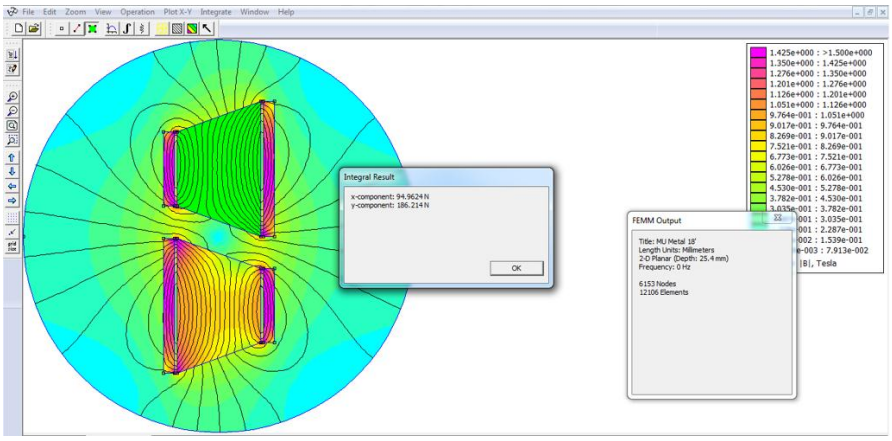

Figure 12. The results of double-sided shielding with 5mm MU Metal Thickness

ISSN (Print): 2413-5267
ISSN (Online): 2706-9966

The cumulative (F_x) was calculated under some considerations of double-sided shield which results in diminishing (F_x) to approximately zero at *a* and *b* positions shown in Figure (13). Position *m* represents fully contact situation between magnets at which (F_x) is maximum. Figure (14) presents an estimation drawing of (F_x - x) relation, where x is the traveling distance associated to the movable magnet. The relationship supposed to be linear as observed from previous results.

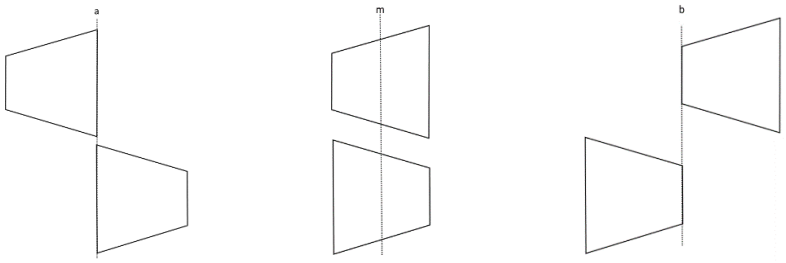

Figure 13. Representation of the movable magnet positions while movement

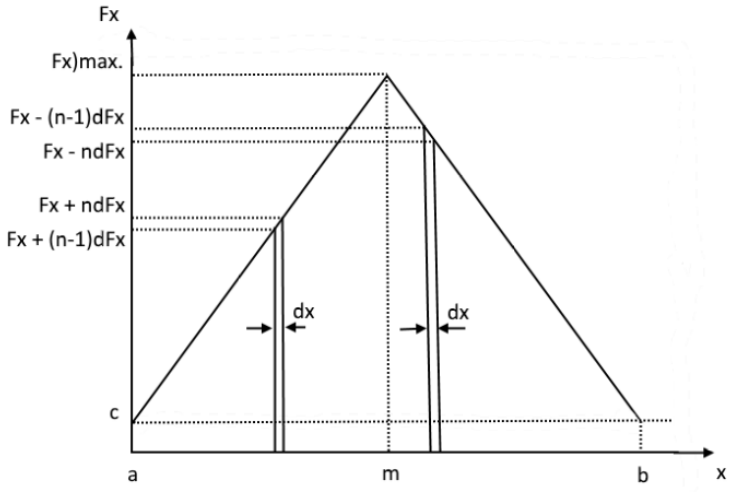

Figure 14. Estimation of (F_x – x) relation

The analysis calculations had been divided into two parts:

Traveling through points *a* and *m* was the first part of the analysis. The Incremental relationship of this part is expressed in the following formula:

$$F_x + ndF_x \qquad \ldots\ldots\ldots \quad (3)$$

where $n=\frac{(Xm-Xa)}{dx}$ is number of differential segments (dx) after which F_x increases incrementally by a differential value equals dF_x.

Therefore;

ISSN (Print): 2413-5267
ISSN (Online): 2706-9966

$$F_x + \frac{(Xm-Xa)}{dx} dF_x \quad \ldots\ldots\ldots \quad (4)$$

The linear relationship of this part can be formulated as the following:

$$F_x = \frac{\Delta Fx}{\Delta x} x + C_1 \quad \ldots\ldots\ldots \quad (5)$$

The derivative of Eqn. (5) was found in order to express dF_x,

$$dF_x = \frac{\Delta Fx}{\Delta x} dx \quad \ldots\ldots\ldots \quad (6)$$

By substituting Eqns. (5 and 6) into Eqn. (4) and taking the limited integration of the found formula, an expression of the first part cumulative F_x (Eqn. 7) is derived as;

$$\int_a^m (Fx + \frac{(Xm - Xa)}{dx} dFx) dx$$

$$\int_a^m (\frac{\Delta Fx}{\Delta x} x + C_1 + \frac{(Xm-Xa)}{dx} (\frac{\Delta Fx}{\Delta x} dx))\, dx$$

$$\frac{\Delta Fx}{\Delta x}(\frac{x^2}{2} + (Xm - Xa)x) + C_1 X \Big|_a^m \quad \ldots\ldots\ldots \quad (7)$$

Moving through points *m* and *b* was the second part of the analysis. The decremental relationship of this part is expressed in the following formula:

$$F_x - ndF_x \quad \ldots\ldots\ldots \quad (8)$$

where $n=\frac{(Xb-Xm)}{dx}$ is number of dx differential segments after which F_x gradually decreases by a differential value equals dF_x.

Thus;

$$F_x - \frac{(Xb-Xm)}{dx} dF_x \quad \ldots\ldots\ldots \quad (9)$$

The linear relationship of this part can be expressed as follows:

$$F_x = \frac{\Delta Fx}{\Delta x} x + C_2 \quad \ldots\ldots\ldots \quad (10)$$

The derivative of Eqn. (10) was determined in order to express dF_x,

$$dF_x = \frac{\Delta Fx}{\Delta x} dx \quad \ldots\ldots\ldots \quad (11)$$

By substituting Eqns. (10 and 11) into Eqn. (9) and taking the limited integration of the found formula, an expression of the second part cumulative F_x (Eqn. 12) is derived as;

ISSN (Print): 2413-5267
ISSN (Online): 2706-9966

$$\int_{m}^{b}(Fx - \frac{(Xb - Xm)}{dx}dFx)dx$$

$$\int_{m}^{b}(\frac{\Delta Fx}{\Delta x}x + C_2 - \frac{(Xb-Xm)}{dx}(\frac{\Delta Fx}{\Delta x}dx))\,dx$$

$$\frac{\Delta Fx}{\Delta x}(\frac{x^2}{2} - (Xb - Xm)x) + C_2X\Big|_{m}^{b} \quad \ldots\ldots\ldots \quad (12)$$

Therefore, the total cumulative F_x (Eqn. 13) can be stated as;

$$\frac{\Delta Fx}{\Delta x}(\frac{x^2}{2} + (Xm - Xa)x) + C_1X\Big|_{a}^{m} + \frac{\Delta Fx}{\Delta x}(\frac{x^2}{2} - (Xb - Xm)x) + C_2X\Big|_{m}^{b}$$

$\ldots\ldots\ldots$ (13)

It is worth to say that both Eqns. (7 and 12) yield the same value of the cumulative F_x due to symmetry.

Torque (T) and work done (W) were calculated for NdFeB 52 MGOe at the same simulated optimum parameters. First of all, the relation of (F_x –x) was graphed (Figure 15) under some assumptions had been taken which were F_x= 10 N at both positions (x= 0 and x= 37.66 mm). Then C_1 and C_2 were calculated as 10 and 156 respectively. The total cumulative F_x in this case was calculated by using the simulation results and substituting into Eqn. (13) as 4500 N. By substituting this value into Eqn. (2), T and W can be expressed in terms of the radius (r) as,

$$W = 2 \times 4500r \times 8 \times \frac{\pi}{4} \quad \ldots\ldots\ldots \quad (14)$$

where n= 8 and $\theta = \frac{\pi}{4}$

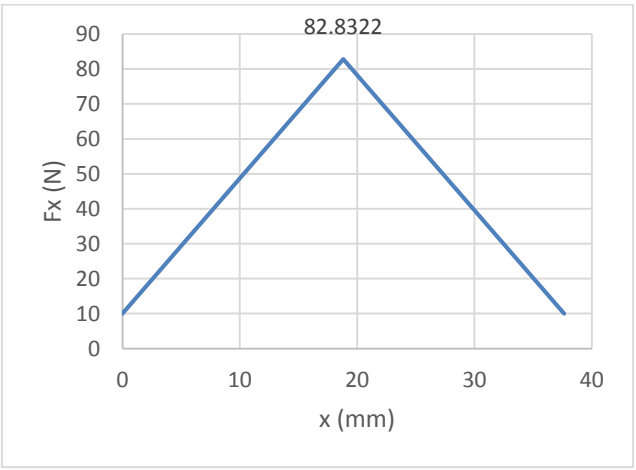

Figure 15. The Cumulated F_x estimation for NdFeB 52 MGOe

ISSN (Print): 2413-5267
ISSN (Online): 2706-9966

Work done was estimated in relation with number of the motor cells under assumption of (r = 20cm). The results were summarized in Table (6), and graphically illustrated in Figure (16).

Table 6. Work done calculations vs. number of the motor cells

Number of the motor cells	Number of disks	Work done (J)
1	1 Stationary/2 Movable	11309.73355
2	2 Stationary/3 Movable	22619.46711
3	3 Stationary/4 Movable	33929.20066
4	4 Stationary/5 Movable	45238.93421
5	5 Stationary/6 Movable	56548.66776

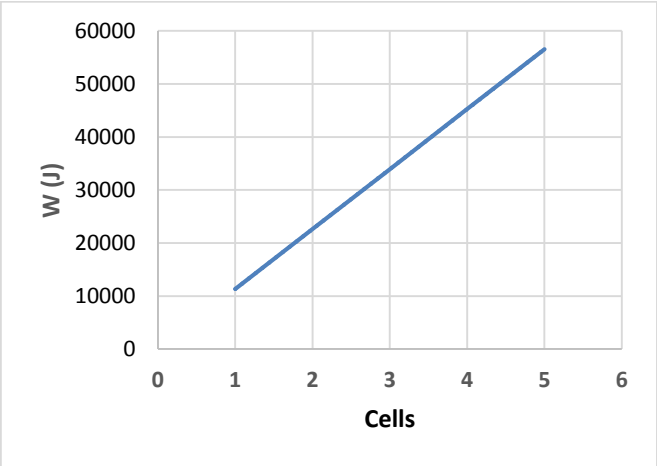

Figure 16. Variation of W with number of cells

4. Discussion

A steady increase in (F_x) value as the input value of (Φ) increases until reached its peak at ($\Phi = 109.7^0$) to fall after that at approximately the same rate. It is worth to say that there is no (F_x) when (Φ) is equal to zero, and it starts to appear at any further values of (Φ). The simulation results obtained under some dimensional constrains of (L), (M) and (Ds) whereas (S) was free to change as (Φ) changes had taken place. Therefore, the magnet's size was subjected to decrease throughout the simulation and that could be the reason behind the subsequent falling of (F_x). As can be seen, (F_x) decreased drastically when (Ds) had been gradually increased. The simulation had been initially carried out at (Ds = 1mm) as a starting point, and (F_x) was maximum at this point. However, its value would obviously be larger at any value of (Ds) smaller than 1mm. interestingly, (F_x) was linearly related to (L) and almost irrelevant relation whatever the depth changes had been made. However, (F_x) increased linearly as (M) had gone up at all the simulated values of depth. Moreover, the analysis and

ISSN (Print): 2413-5267
ISSN (Online): 2706-9966

simulation indicate that a substantial rise in (F_x) observed whenever the changes in depth had been carried out. The results state that Neodymium and Samarium–cobalt magnets performance was the best comparing with other types. Nevertheless, these results are limited only on the available magnetic materials in the materials library of FEMM software. Other magnetic materials could be added to the library and shown close results. Regarding to shielding, the findings were quite unexpected and suggest that whenever the thickness of MU Metal in case of single-sided shield increases, (F_x) increases whereas (F_y) remains constant. The reason behind could be the additional repulsive force that introduced in the shielded side of the stationary magnet as a result of increasing flux density. The same goes for the case of double-sided shield with a small difference of (F_y) values that slightly alter comparing with (F_x) due to the size of magnet's poles difference. Nevertheless, the saturation situation seems to be achievable at MU Metal thickness in the range of 5 to 10 mm for both cases of shielding. The results show a substantial energy could be obtained by repeating the cells in a linear pattern; however, more expected energy would be gained at larger magnet's size and disk's radius. Furthermore, angular velocity and acceleration can be calculated when specifying materials.

5. Conclusion

It is the time to renew primary energy sources toward sustainability for a clean environment. Many alternatives around the world could be investigated to be high performance energy sources. Besides well-known renewable energy sources such as wind, solar, and hydropower, free energy sources such as perpetual motion machines and permanent magnetic motors might be good choices. Although an excessive work has been done in this area, a few reached satisfactory outcomes. Investigation and simulation of the new design proposed in this research by taking into account types of magnetic materials show a gigantic energy could be obtained by using small permanent magnets. In addition, the produced energy might be multiplied to get huge values by increasing number of cells and the size of magnets. However, neodymium magnets which are so expensive provided optimal simulation results. Hence a conflict arises within their availability and supplementary.

References

Baltzis K.B. (2010). The finite element method magnetics (FEMM) freeware package: May it serve as an educational tool in teaching electromagnetics. *Journal Education and Information Technologies*, 15(1): 19–36.

Furlani E.P. (2001). *Permanent magnet and electromechanical devices: materials, analysis, and applications*, 2nd edition. Academic press, New York.

Jiles D.C. (1991). *Introduction to Magnetism and Magnetic Materials*, 2nd ed., CRC press.

Kelly P.J. (2010). *Practical Guide to Free-Energy Devices*. Available online at: [http://www.free-energy-info.com/PJKbook.pdf].